Chemical Science

ROYAL SOCIETY OF CHEMISTRY

EDGE ARTICLE

View Article Online
View Journal | View Issue

Open Access Article. Published on 19 February 2024. Downloaded on 1/20/2026 12:47:57 PM.
This article is licensed under a Creative Commons Attribution-NonCommercial 3.0 Unported Licence.

Check for updates

Cite this: *Chem. Sci.*, 2024, **15**, 4510

All publication charges for this article have been paid for by the Royal Society of Chemistry

Long live(d) $CsPbBr_3$ superlattices: colloidal atomic layer deposition for structural stability†

Victoria Lapointe,[a] Philippe B. Green,[b] Alexander N. Chen,[b] Raffaella Buonsanti[b] and Marek B. Majewski *[a]

Received 11th December 2023
Accepted 18th February 2024

DOI: 10.1039/d3sc06662b

rsc.li/chemical-science

Superlattice formation afforded by metal halide perovskite nanocrystals has been a phenomenon of interest due to the high structural order induced in these self-assemblies, an order that is influenced by the surface chemistry and particle morphology of the starting building block material. In this work, we report on the formation of superlattices from aluminum oxide shelled $CsPbBr_3$ perovskite nanocrystals where the oxide shell is grown by colloidal atomic layer deposition. We demonstrate that the structural stability of these superlattices is preserved over 25 days in an inert atmosphere and that colloidal atomic layer deposition on colloidal perovskite nanocrystals yields structural protection and an enhancement in photoluminescence quantum yields and radiative lifetimes as opposed to gas phase atomic layer deposition on pre-assembled superlattices or excess capping group addition. Structural analyses found that shelling resulted in smaller nanocrystals that form uniform supercrystals. These effects are in addition to the increasingly static capping group chemistry initiated where oleic acid is installed as a capping ligand directly on aluminum oxide. Together, these factors lead to fundamental observations that may influence future superlattice assembly design.

Introduction

Metal halide perovskite nanocrystals (PNCs) are promising materials for many applications such as photovoltaics,[1] photodetectors,[2] photocatalysts,[3] and scintillators[4] due to their diverse and tunable optoelectronic properties governed by their composition and stabilized by a wide breadth of surface capping groups.[5–7] Ordered PNC self-assembly under slow solvent evaporation leads to superlattice (SL) formation where the individual PNCs can be considered "atoms" and the extended structure leads to micron-sized cubic supercrystals.[8,9] The morphology of the extended structure, as in standard crystal formation, is dictated by a balance of entropy and enthalpic contributions and variations in the constituent "atoms" as well as their surface composition which can lead to different structures and supercrystal stoichiometry (ranging from primary crystal structures such as cubic, BCC, and FCC to more complex binary systems and beyond that are isostructural with known atomic lattices).[9–12] These are characterized through the observation of crystallographic multilayer diffraction where investigating fundamental structural properties and self-assembly processes remains important to augment our understanding of such superstructures.[8,12–15]

It is well understood in PNCs that the capping ligands undergo dynamic surface chemistry and therefore can detach from the crystal surface. This phenomenon not only increases the surface defects but also affects their self-assembly and structural integrity much like the imperfections found in even the most carefully prepared atomic crystals.[1,2,6,7,16] Even under inert atmospheres SLs assembled from PNCs are only stable for 4–5 days before showing signs of structural aging.[16]

Colloidal atomic layer deposition (c-ALD) has been found to stabilize nanocrystals against moisture, polar solvents, and ligand dynamicity through the deposition of subnanometer metal oxide shells under mild, colloidal conditions.[17–19] Growth of metal oxide layers, more specifically aluminum oxide (AlO_x) shells, onto the surface of nanocrystals is carried out by sequentially adding a reactive metal precursor (trimethylaluminum, TMA) and pure oxygen to a dilute colloid at room temperature.[18,19]

As a strategy to stabilize PNC superlattices, we sought to grow a protective matrix on their constituent PNC building blocks that would render the final superstructure structurally stable. In this work, we report on the use of c-ALD as a method to grow AlO_x shells on PNCs without affecting their self-assembly into supercrystals (Scheme 1). We also demonstrate that the c-ALD treatment increases the overall

[a]Department of Chemistry and Biochemistry, Centre for NanoScience Research, Concordia University, 7141 Sherbrooke Street West, Montreal, Quebec, H4B 1R6, Canada. E-mail: marek.majewski@concordia.ca

[b]Laboratory of Nanochemistry for Energy, Institute of Chemical Sciences and Engineering, École Polytechnique Fédérale de Lausanne, Sion, CH-1950, Switzerland

† Electronic supplementary information (ESI) available: Experimental procedures, photoluminescence spectroscopy, UV-vis spectroscopy, X-ray photoelectron spectroscopy, STEM-EDS, SEM, TEM, powder X-ray diffraction, and ^{1}H NMR spectra. See DOI: https://doi.org/10.1039/d3sc06662b

© 2024 The Author(s). Published by the Royal Society of Chemistry

Open Access Article. Published on 19 February 2024. Downloaded on 1/20/2026 12:47:57 PM.
This article is licensed under a Creative Commons Attribution-NonCommercial 3.0 Unported Licence.

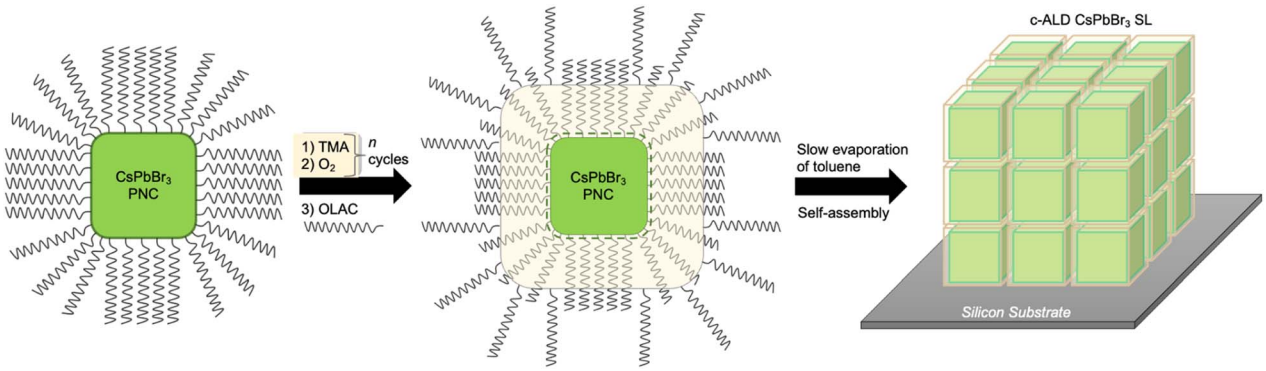

Scheme 1 Colloidal atomic layer deposition process followed by SL formation through slow evaporation.

photoluminescence quantum yields and average radiative lifetimes of both the PNCs and corresponding SLs. We show that c-ALD treated $CsPbBr_3$ PNCs form SLs that are structurally more stable for a period of 25 days under nitrogen atmosphere as compared to their untreated counterparts. The c-ALD treated $CsPbBr_3$ SLs also demonstrate tunability through controlling the AlO_x shell thickness deposited onto the PNCs before self-assembly. In contrast, growing AlO_x by traditional gas phase ALD destroys them.

Results and discussion

Characterization of c-ALD treatment on $CsPbBr_3$ PNCs

$CsPbBr_3$ PNCs were prepared by using a scaled-up version of the typical hot-injection synthesis as reported by Protesescu *et al.*[7] The c-ALD procedure was applied as first reported by Loiudice *et al.* adjusted according to the concentration of the colloidal PNC solution (see ESI for Experimental details†).[17–20] Two different shelling methods were tested: shelling with TMA and O_2 only, and shelling with TMA, O_2, and oleic acid (OLAC) added as a terminating group on the last cycle (see ESI† for more details on the synthetic procedure). Previous studies indicate that TMA nucleates onto PNCs surface *via* OLAC and *via* hydroxyl groups. Upon this surface reaction, oxygen is pulsed into the colloidal solution to form the AlO_x shells.[18,19,21,22] Both c-ALD treated PNCs were characterized, however samples with AlO_x shelling without OLAC termination suffered from low stability as colloids (see ESI, Fig. S1†), therefore the OLAC terminated c-ALD treated $CsPbBr_3$ PNCs were carried forward for our investigations. For the purposes of this discussion the shelled PNCs are labeled as n c-ALD OLAC where there were $(n-1)$ AlO_x cycles (TMA/O_2 cycles) and a final AlO_x-OLAC cycle (TMA/OLAC); the n values studied and reported here are 1, 3, 5, 7, and 10 alongside an untreated-$CsPbBr_3$ PNC solution ($n = 0$).

A careful analysis of the optical properties of the untreated and c-ALD treated OLAC terminated $CsPbBr_3$ PNCs was carried out. The untreated $CsPbBr_3$ PNCs, after purification and filtration through a 2 μm PTFE syringe filter, were analyzed by UV-vis absorbance and photoluminescence (PL) spectroscopy, photoluminescence quantum yield (PLQY), and time-resolved photoluminescence (TRPL) measurements. From these data, the parent $CsPbBr_3$ PNCs had a calculated bandgap of 2.51 eV (498 nm, as determined by taking the λ_{max} of the excitonic peak in the UV-vis absorbance spectrum), a PL maximum peak (λ_{em}) at 513 nm with a full width at half maximum (FWHM) of 22 nm, PLQY of 44% and average PL radiative lifetime of 22.8 ns (Fig. 1A, B and Table S1†). TEM micrographs show low size dispersity and uniform cubic PNCs with average particle size of 9.70 ± 1.16 nm (Fig. 2C inset and S2†).[15,23]

Post-c-ALD treated and OLAC terminated $CsPbBr_3$ PNCs showed no significant changes in calculated bandgaps or λ_{em}, and only a slight increase in the PL FWHM values, all outcomes that are comparable to previously reported results (Fig. 1A, S3 and Table S1†).[17–19] Notably, we observed an overall increase in PLQY (44% up to 62%) and average PL lifetimes (22.8 ns up to 29.5 ns) after shelling with AlO_x as successive shells passivate defects on the surface of the PNCs (Fig. 1B, S4 and Table S1†).[18] These data confirm that the structural integrity of the PNCs was preserved in the course of the c-ALD treatment and emphasized that c-ALD is a valid strategy for enhancing radiative decay in PNCs.

The attenuated total reflectance Fourier transform infrared spectra (ATR-FTIR, Fig. 1C) of the treated $CsPbBr_3$ PNCs show the four bands corresponding to vibrational modes of the AlO_x shells (1260, 1094, 1023, 801 cm^{-1}) alongside the expected capping group vibrational modes [from oleylamine only: ν(N–H) ~3165 cm^{-1}, δ(N–H) 1534–1625 cm^{-1}; from oleic acid only: ν(C=O) ~1706 cm^{-1}, ν(COO–) 1540–1465 cm^{-1}; from both capping groups: ν(C–H) 3010–2850 cm^{-1}, δ(C–H) 1465–1375 cm^{-1}, ν(C=C–H) 2945 cm^{-1}, ν(C=C) 965 cm^{-1}].[19,24] From these data, we conclude that using vibrational spectroscopy in these samples is not an accurate measurement of shell thickness, but does confirm that the existing surface capping ligands are embedded within the AlO_x shell. The presence of an AlO_x shell is also confirmed through X-ray photoelectron spectroscopy (XPS) analysis as the Al 2s core-level regions only appear after c-ALD treatment while maintaining the other core level regions of the other elements within the $CsPbBr_3$ PNCs (Fig. 1D and S5†). The scanning transmission electron microscopy (STEM) micrographs and energy dispersive X-ray spectroscopy (EDS) elemental mapping of 5 c-ALD OLAC PNCs demonstrate that the Al is spatially correlated with Pb, suggesting the

Open Access Article. Published on 19 February 2024. Downloaded on 1/20/2026 12:47:57 PM.
This article is licensed under a Creative Commons Attribution-NonCommercial 3.0 Unported Licence.

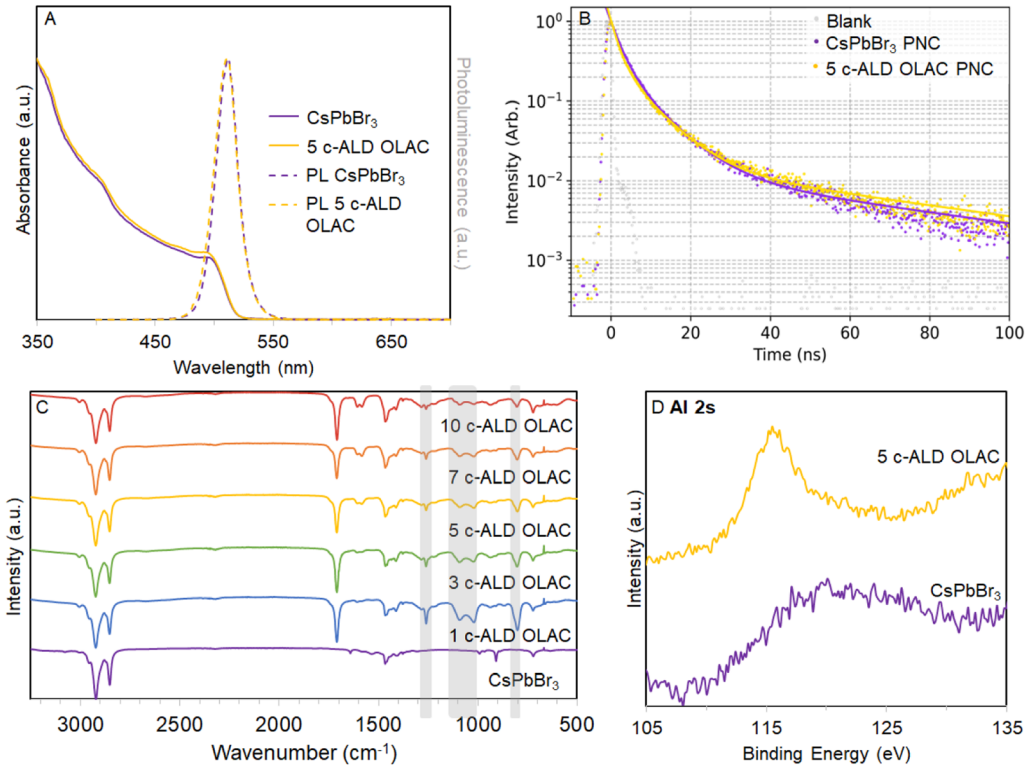

Fig. 1 (A) UV-vis absorbance (solid lines) and photoluminescence (dotted line) spectra of $CsPbBr_3$ and of 5 c-ALD OLAC PNCs where photoluminescence spectra were collected at $\lambda_{ex} = 365$ nm and room temperature. (B) Time-resolved photoluminescence decay traces and corresponding fits of $CsPbBr_3$ and of 5 c-ALD OLAC PNCs in toluene, $\lambda_{ex} = 455$ nm laser at room temperature. (C) FTIR spectra with highlighted AlO_x vibrational modes of untreated and treated $CsPbBr_3$ PNCs, (D) XPS spectra of untreated $CsPbBr_3$ and 5 c-ALD OLAC PNCs for the Al 2s core-level region.

formation of an alumina shell and the absence of homogeneously nucleated alumina (Fig. S6†). Additionally, ^{1}H-NMR, diffusion ordered spectroscopy (DOSY), and Nuclear Overhauser Effect spectroscopy (NOESY) spectra are consistent with bound OLAC when comparing the 5 c-ALD OLAC PNCs to untreated $CsPbBr_3$ PNCs (Fig. S7 and 8†).[17]

Optical and structural characterization of $CsPbBr_3$ SLs

The self-assembly of SLs was carried out through a modification of the procedure reported by Baranov *et al.* (Scheme 1).[16] Post-c-ALD PNCs were dried under nitrogen, redispersed in 0.3 mL of toluene and filtered using a 2 μm PTFE syringe filter before a 30 μL aliquot was drop cast onto a clean 1 cm × 0.5 cm silicon substrate. The solvent was left to slowly evaporate overnight in a nitrogen filled glovebox. It was found that the c-ALD treated $CsPbBr_3$ PNCs had to be terminated with OLAC for the shelled PNCs to remain stable as a colloid and to self-assemble into SLs as determined by θ–θ powder X-ray diffraction (PXRD, Fig. S1,† and 2A). This is expected, as it has been established that surface ligand interactions dictate colloidal stability but also impact self-assembly.[13,25] Moreover, the inability for c-ALD treated PNCs (without OLAC termination) to form simple cubic SLs may indicate surface shell anisotropy or deviation from a purely cubic shape to one that is becoming spherical that disfavors purely face-to-face packing.[11] Specifically, the long carbon chains provided by the OLAC terminated PNCs undergo van der Waals interactions during the slow evaporation process for the SL formation, thus determining the repeating distance between the PNCs within the SL structure while simultaneously controlling the supercrystal shape.[26] In all cases, at room temperature, the solid state PL, and TRPL analyses indicated that SLs assembled from shelled PNCs remained similar to those assembled from untreated PNCs with slight decreases in PLQY and average TRPL lifetimes (Fig. S9, 10 and Table S2†).[18,23,27]

A detailed structural analysis was performed after the untreated and c-ALD OLAC treated $CsPbBr_3$ PNCs self-assembled into SLs through PXRD, scanning electron microscopy (SEM), and transmission electron microscopy (TEM) (Fig. 2). The PXRD diffractograms show the expected reflections for $CsPbBr_3$ PNC SLs with periodically spaced satellite peaks from the (110), (1$\bar{1}$0), and (002) planes in the splitting of the reflection at 15° 2θ and the (220), (2$\bar{2}$0), and (004) planes at 30° 2θ that originate from the preferential alignment of the PNCs with the silicon substrate planes, as previously reported for $CsPbBr_3$ SLs (Fig. 2A).[8,16,28] Within SLs, the PNCs act as diffraction gratings and X-rays are diffracted by the spacing of the PNCs from each other and their own atomic planes, allowing for splitting or fringes to occur at lower angles (15° 2θ). SLs also contain continuous disorder, related to variability in PNC-to-

 © 2024 The Author(s). Published by the Royal Society of Chemistry

Open Access Article. Published on 19 February 2024. Downloaded on 1/20/2026 12:47:57 PM.
This article is licensed under a Creative Commons Attribution-NonCommercial 3.0 Unported Licence.

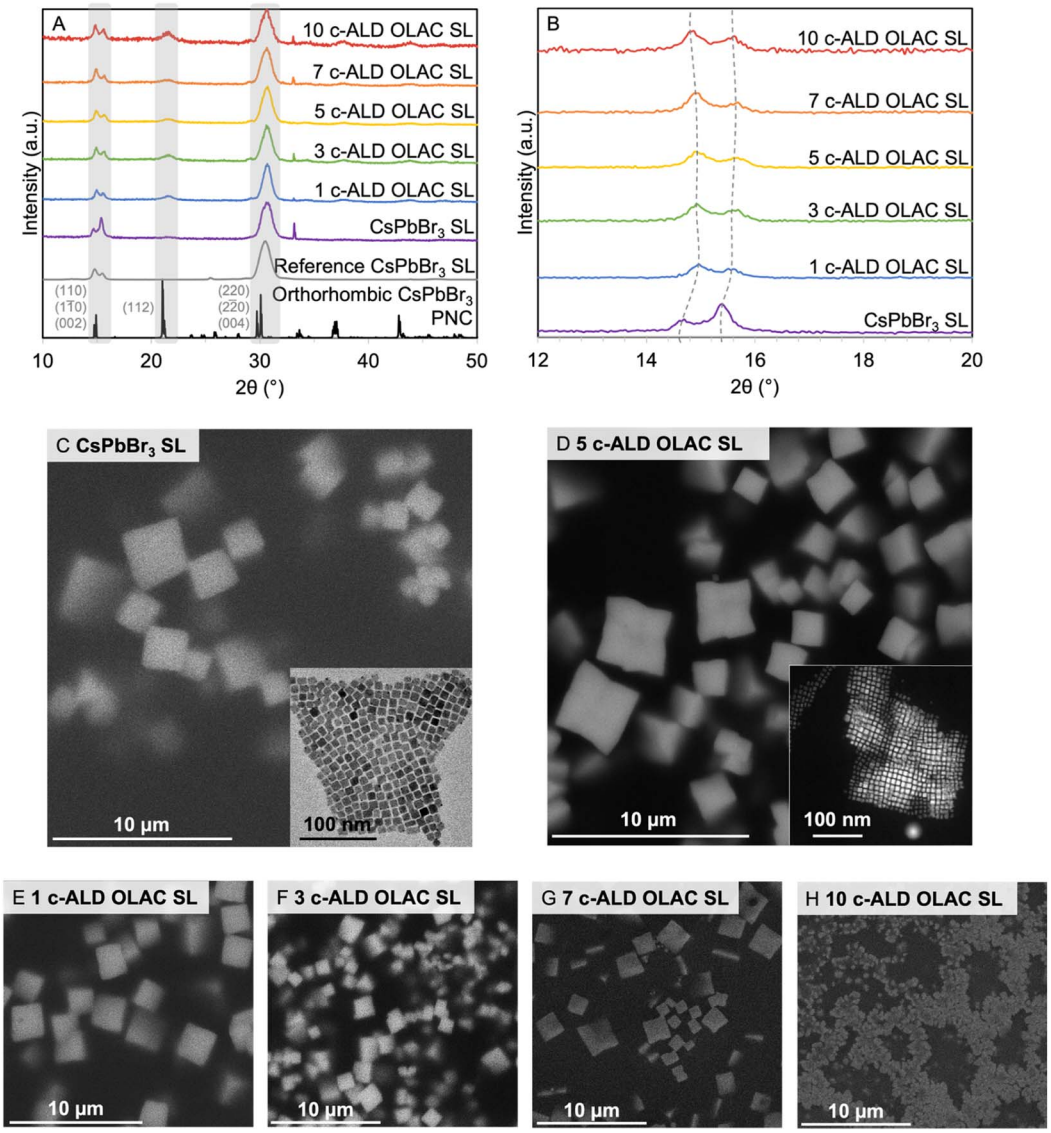

Fig. 2 (A) PXRD diffractograms of SLs constructed from untreated and c-ALD OLAC treated $CsPbBr_3$ PNCs (reference pattern for orthorhombic $CsPbBr_3$ PNCs from ICSD 97851, reference SL pattern from ref. 23), and (B) isolation of splitting at 15° 2θ. (C) SEM and (inset) TEM micrographs of $CsPbBr_3$ SLs and PNCs, respectively, (D) SEM and (inset) HAADF-STEM micrographs of 5 c-ALD OLAC SL and PNCs, respectively, (E) SEM-EDS mapping of 5 c-ALD OLAC SLs, and (F–I) SEM micrographs of corresponding c-ALD OLAC treated $CsPbBr_3$ SLs.

PNC spacing due to the thickness of organic capping group layers, and discrete disorder, relating to PNC monodispersity and inevitable misalignment of PNCs due to disordered sites, as observed through smoother and broader reflections at higher angles (30° 2θ).[8,28,29] In our data, the reflection at 33.5° 2θ corresponds to the silicon substrate (Fig. 2A). The lack of broad reflections at *ca.* 20° 2θ typically associated with amorphous AlO_x signifies that the AlO_x shells are thin and do not affect the crystallinity of the PNCs or SLs.[30] Elemental mapping in SEM (SEM-EDS) also demonstrates that Al is localized on all PNCs across all supercrystals (Fig. 2E and S11†).

The SL periodicity (Λ) and *d*-spacing (d) were estimated from the splitting at 15° 2θ.[29] From this estimation, an overall decrease in Λ for untreated $CsPbBr_3$ (13.15 nm) *versus* 1, 3, 5, 7, 10 c-ALD OLAC samples (14.09 nm, 13.15 nm, 12.33 nm, 11.60 nm, 11.60 nm, respectively) and an overall small decrease in d for untreated $CsPbBr_3$ (0.5888 nm) *versus* 1, 3, 5, 7, 10 c-ALD OLAC samples (0.5793 nm, 0.5802 nm, 0.5776 nm, 0.5785 nm, 0.5819 nm, respectively) was calculated (Fig. 2B and Table S3†). Increasing the number of shells also leads to a decrease in crystallinity and emergence of reflections associated with disordered free PNCs not part of a supercrystal (22, 34, 38, and 44° 2θ) as observed in the 10 c-ALD OLAC diffractogram. From analysis of the PXRD data alone, it appears that SLs assembled from PNCs with AlO_x shells may exhibit an overall "contraction" of the SL assembly until 7 AlO_x shells.

Structural information obtained by PXRD was confirmed by SEM and TEM. SEM micrographs confirm the existence of SLs of $CsPbBr_3$ and 1, 3, 5, 7 c-ALD OLAC samples but small and irregular SLs for 10 c-ALD OLAC (Fig. 2C, D and F–I). This result

Open Access Article. Published on 19 February 2024. Downloaded on 1/20/2026 12:47:57 PM. This article is licensed under a Creative Commons Attribution-NonCommercial 3.0 Unported Licence.

indicates that increased AlO_x shells may no longer favor self-assembly as the increase in AlO_x shelling may result in more inhomogeneity on the PNC surface creating stacking disorder within the SL structure.[18,29] Discrete $CsPbBr_3$ supercrystals show an average size of 2.21 ± 0.45 μm (Fig. 2C inset) while those from c-ALD treated PNCs had sizes of 2.10 ± 0.48 μm, 1.60 ± 0.31 μm, 1.83 ± 0.41 μm, and 1.63 ± 0.49 μm for 1, 3, 5, 7 c-ALD OLAC SLs, respectively (Fig. 2C, D and F–I). The PNC sizes and (edge-to-far edge) PNC-to-PNC distances were then also calculated from the TEM micrographs obtained for the untreated $CsPbBr_3$ and the 5 c-ALD OLAC samples. However, the TEM micrographs of the $CsPbBr_3$ samples show an average PNC size of 9.70 ± 1.16 nm and a PNC-to-PNC distance of 11.71 ± 1.00 nm (Fig. 2C inset, S2 and S12†) whereas the 5 c-ALD OLAC samples were found to have an average PNC size of 8.92 ± 1.35 nm and a PNC-to-PNC distance of 11.01 ± 1.01 nm (Fig. 2D inset and S13†). Although, these values are qualitatively consistent with the results from the PXRD, where average PNC-to-PNC distances agree somewhat with the calculated SL periodicities, it may indicate that the decrease in these values is due to a decrease in PNC size after c-ALD treatment instead of a "contraction" between PNCs. The smaller average PNC size post-c-ALD treatment may correspond to the removal of the original surface capping groups (such as OLAM) and a concomitant loss of the outermost layer(s) of PNC ions, however, c-ALD also passivates surface defects (as confirmed by increasing PLQYs, *vide supra*). From the present data it is difficult to conclude on the ultimate nature of the final outer shell of the c-ALD treated PNCs. Based on previous work, we hypothesized that the c-ALD initiates shelling *via* reaction of the TMA with OLAC and, possibly, hydroxyl groups on the surface of the PNCs.[17–19,21,22,31] The nucleation clusters then interconnect to form a homogenous monolayer.[22,31] As the growth continues, the same amount of TMA was added per each cycle. Thus, beyond a certain number of cycles, we expect the homogeneity and compactness of the AlO_x layers to decrease.[31] As a result, the overall size of the AlO_x treated PNCs should be more homogeneous with lower numbers of AlO_x shells. These result in "tighter" packing within their respective SLs. Meanwhile, the increased inhomogeneity and lower density of the shell for higher numbers of c-ALD cycles results in softer AlO_x treated PNCs and, thus, in a lower packing density forming decreasingly cubic SLs (as evidenced from the PXRD, Fig. 2A).[11,28] It appears that the c-ALD treated PNCs act as hard cubes leading to face-to-face contact between neighboring particles with a balance of grafting density and interdigitation of surface ligands (as indicated by the TEM data).[11,25] Moreover, as the edge length decreases a decreased lattice constant is expected. Adding too many shells leads to the formation of softer cubes that may deviate from a purely cubic structure with increasingly ligand-rounded edges, perturbed surface ligand grafting densities (outside of 1 chains per nm^2) and leading to different packing orientations (and the formation of corresponding ligand vortices) not allowing for the formation of purely simple cubic lattices as observed in the 10 c-ALD OLAC samples.[11,25] Significantly, SEM micrographs also reveal that the c-ALD OLAC treated $CsPbBr_3$ SLs are much more homogenously sized than the untreated $CsPbBr_3$ SLs that showed areas of "amorphous" unassembled PNCs around the cubic SLs (Fig. S14†).

To confirm these observations and to test if the c-ALD technique allowed for versatile capping groups to be added onto the surface of PNCs and confirm the nature of the packing in the SL, a molar equivalent of didodecyldimethylammonium bromide (DDAB) was used to replace OLAC in a c-ALD synthesis. DDAB, specifically the DDA cation, is a stable hydrophobic monolayer for functionalizing negatively charged surfaces.[32] Since 5 c-ALD OLAC SLs showed the best structural stability results, the same number of c-ALD cycles was used in this procedure to yield 5 c-ALD DDAB PNCs that demonstrated similar absorbance and photoluminescence spectra as compared to the parent PNCs. Notably, the PLQY increased to 98% and an increased average lifetime was measured by TRPL (22.9 ns as colloidal PNCs and 28.5 ns as SLs) a finding that agrees with the increase in PLQY and matching previous reports (Fig. S15–18 and Table S4†).[23] Inspecting the morphology of 5 c-ALD DDAB SLs confirms that these samples result in cubic SLs (Fig. S19†). Using the same set of calculations as for the previous SLs, Λ and d were calculated to be 16.43 nm and 0.5879 nm, respectively, demonstrating an opposite trend to the c-ALD OLAC samples (Table S3†). From TEM an average PNC size of 10.81 ± 1.13 nm and PNC-to-PNC distance of 13.16 ± 1.45 nm was determined (Fig. S19 and 20†). The chain length of DDAB (1.7 nm) being longer than OLAC (1.5 nm) together with DDAB being somewhat sterically hindered owing to two alkyl groups within its structure;[23,33] may increase the soft particle behaviour for these capped PNCs. From SEM, it was found that the 5 c-ALD DDAB SLs were on average 0.32 ± 0.10 μm in size, smaller than untreated and c-ALD OLAC treated $CsPbB_3$ SL samples. Nevertheless, c-ALD allows the facile incorporation of different capping groups to study the effects on SL formation.

On the stability of c-ALD treated SLs

We studied their structural integrity of $CsPbBr_3$ SLs over the course of many days through PXRD and SEM to quantify the effects of the c-ALD treatment. To do so, the SL samples were stored in a nitrogen filled glovebox, and only removed for PXRD and SEM analysis. The untreated $CsPbBr_3$ SL diffractogram shows a shift in the intensity reflection splitting ratios followed by a decrease of the splitting at the 15° 2θ over the course of 5 days (Fig. 3A). This loss of ordered structure is confirmed *via* SEM where the once cubic, and oriented SLs begin to look globular and randomly oriented (Fig. 3C and D). After 5 days, this sample, under reduced magnification, appeared "amorphous" with a distinct loss of superlattice structure (Fig. 3E). The 5 c-ALD DDAB SLs only appeared stable for less than 6 days when observing the splitting at the 15° 2θ reflection in PXRD and the SEM micrographs (Fig. S19†). The c-ALD OLAC treated SLs maintained the splitting of the 15° 2θ reflection beyond 5 days, especially in the 5 c-ALD OLAC sample that still showed signs of the splitting for 22 days (Fig. 3B). All treated SLs also began exhibiting additional splitting at the 30° 2θ reflection alongside strong reflections matching those of PNCs; this may point to the formation of better aligned atomic planes within

 © 2024 The Author(s). Published by the Royal Society of Chemistry

Open Access Article. Published on 19 February 2024. Downloaded on 1/20/2026 12:47:57 PM.
This article is licensed under a Creative Commons Attribution-NonCommercial 3.0 Unported Licence.

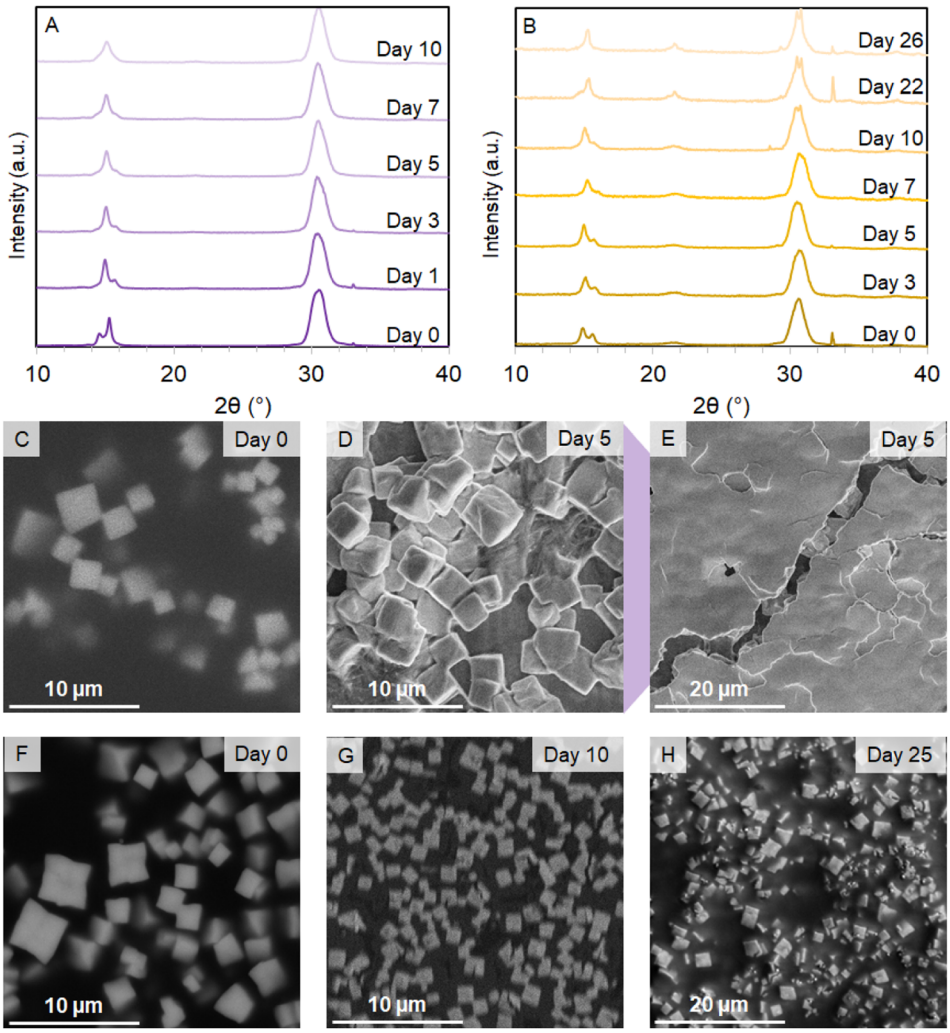

Fig. 3 Time-resolved PXRD diffractograms of (A) untreated $CsPbBr_3$ SL and (B) 5 c-ALD OLAC SL. SEM micrographs of (C–E) untreated $CsPbBr_3$ SL ((E) is a lower magnification image of (D)) and (F–H) of 5 c-ALD OLAC SL documenting the aging process, where all micrograph except (H) were taken in secondary electron mode ((H) was taken in Topo A + B mode). The $CsPbBr_3$ SLs were stored under ambient room light in a nitrogen-filled glovebox until subsequent PXRD and SEM analyses where the SLs were exposed to ambient conditions for the duration of the measurements.

the SLs before deteriorating into individual PNCs on aging (Fig. 3B).[8,28] The SEM micrographs of the 5 c-ALD OLAC SLs confirmed that the SLs retained some structural integrity until day 25, it was only at day 30 that the sample showed clear signs of complete SL break down where the larger SLs are broken down into smaller, brighter cubic domains in the SEM micrograph (Fig. 3F–H and S21†).[16] We also note that samples became sensitive to destruction by the electron beam likely due to the charge build-up from the PNCs within the insulating AlO_x shell, so SEM micrographs were collected with lower magnification. Nonetheless, the c-ALD shell was demonstrated to be crucial for the stability of $CsPbBr_3$ SLs. This may be due to the fact that these anisotropic shells protect the PNCs with the SL from ambient conditions.[11,25]

In order to verify that c-ALD was in fact the reason for the increase in structural stability for SLs, we also compared gas phase ALD (g-ALD) on pre-assembled $CsPbBr_3$ SLs as well as simply adding extra OLAC to a premade $CsPbBr_3$ SL. The g-ALD required heating (50 °C) and exposing this sample to cycles of gaseous TMA and H_2O (conditions that represent some of the milder AlO_x deposition parameters possible with g-ALD). It is important to consider that the c-ALD layers and the g-ALD layers are not directly comparable, therefore, 25 and 50 cycles of g-ALD were applied to a $CsPbBr_3$ SL sample as a strategy to protect the entire SL from the environment rather than stabilizing individual nanocrystals.[34,35] After PXRD and SEM characterization, it was determined that the SL structures did not survive the harsh conditions together with the formation of a thick amorphous layer of AlO_x demonstrating that c-ALD is the optimal method for protecting the PNCs within the SL formation from aging (Fig. S22 and 23†). To our knowledge, no protocol using g-ALD to shell individual PNCs has been established, hence reinforcing the utility of c-ALD to protect individual SL building blocks.[34,35] Adding extra OLAC to an as-synthesized $CsPbBr_3$ SL

Open Access Article. Published on 19 February 2024. Downloaded on 1/20/2026 12:47:57 PM. This article is licensed under a Creative Commons Attribution-NonCommercial 3.0 Unported Licence.

also revealed no increase in structural stability and by SEM showed aging more rapidly than an untreated $CsPbBr_3$ SL (Fig. S24†). This result might derive from a perturbation of dynamic surface chemistry enabled by an increased amount of OLAC leading to a loss of extended structure.[16,36] This further solidifies the importance of the c-ALD shelling behaviour on the structural stability of the SLs.

Conclusions

We have shown that c-ALD shelled PNCs self-assemble into SLs with higher resistance to structural aging compared to untreated PNCs. As opposed to g-ALD, c-ALD provides structural protection while also allowing for versatility of attached capping groups onto the metal oxide shell surface of these PNCs. By PXRD, SLs assembled from PNCs shelled by c-ALD exhibit a general contraction of the superstructure with a decreasing periodicity together with shrinking PNC-to-PNC distances. While this was not verified through electron microscopy analysis, we note that recently, the Orbifold Topological Model has been adapted to the packing of cubic PNCs.[11,12] Those findings showed that nanocubes generally pack as hard shapes, while the introduction of vortices leads to a breakdown of the hard shape description. Our findings have indicated that c-ALD treated PNCs act as hard cubes up to a certain AlO_x thickness (due to the formation of homogenous shells), where afterwards, surface anisotropy, a (presumed) deviation from the purely cubic shape (AlO_x clusters on the surface of the PNCs), and generally softer behavior leads to a breakdown in superlattice formation. We believe that these results lend some fundamental understanding of the nature of the AlO_x shell that should be further investigated or extended to other oxide shell formation. Ultimately, we anticipate that the use of c-ALD together with the formation of $CsPbBr_3$ SLs may lead to next generation optoelectronic devices.

Data availability

Data generated or analyzed during this study are available from the corresponding author upon reasonable request.

Author contributions

V. L. carried out all experimental work with the support of P. B. G. who mentored on the methods for c-ALD and performed NMR characterization. A. C. collected SEM, STEM and TEM micrographs and corresponding elemental analysis. The manuscript was written through contributions from V. L., P. B. G, R. B. and M. B. M.

Conflicts of interest

There are no conflicts to declare.

Acknowledgements

V. L. and M. B. M. thank the Natural Sciences and Engineering Research Council of Canada (NSERC) [M. B. M. funding: RGPIN-2018-04391], Fonds de Recherche du Québec – Nature et technologies (FRQNT), and Quebec Centre for Advanced Materials (QCAM) for financial support. V. L. thanks NSERC and FRQNT for graduate scholarships. V. L. carried out this work as part of a NSERC Michael-Smith Foreign Study Supplement.

Notes and references

1 E. M. Sanehira, A. R. Marshall, J. A. Christians, S. P. Harvey, P. N. Ciesielski, L. M. Wheeler, P. Schulz, L. Y. Lin, M. C. Beard and J. M. Luther, Enhanced Mobility $CsPbI_3$ Quantum Dot Arrays for Record-Efficiency, High-Voltage Photovoltaic Cells, *Sci. Adv.*, 2017, **3**(10), eaao4204, DOI: 10.1126/sciadv.aao4204.

2 Y. Dong, Y. Zou, J. Song, X. Song and H. Zeng, Recent Progress of Metal Halide Perovskite Photodetectors, *J. Mater. Chem. C*, 2017, **5**(44), 11369–11394, DOI: 10.1039/C7TC03612D.

3 Y.-F. Xu, M.-Z. Yang, B.-X. Chen, X.-D. Wang, H.-Y. Chen, D.-B. Kuang and C.-Y. Su, A $CsPbBr_3$ Perovskite Quantum Dot/Graphene Oxide Composite for Photocatalytic CO_2 Reduction, *J. Am. Chem. Soc.*, 2017, **139**(16), 5660–5663, DOI: 10.1021/jacs.7b00489.

4 F. Carulli, M. He, F. Cova, A. Erroi, L. Li and S. Brovelli, Silica-Encapsulated Perovskite Nanocrystals for X-Ray-Activated Singlet Oxygen Production and Radiotherapy Application, *ACS Energy Lett.*, 2023, **8**(4), 1795–1802, DOI: 10.1021/acsenergylett.3c00234.

5 A. Dey, J. Ye, A. De, E. Debroye, S. K. Ha, E. Bladt, A. S. Kshirsagar, Z. Wang, J. Yin, Y. Wang, L. N. Quan, F. Yan, M. Gao, X. Li, J. Shamsi, T. Debnath, M. Cao, M. A. Scheel, S. Kumar, J. A. Steele, M. Gerhard, L. Chouhan, K. Xu, X. Wu, Y. Li, Y. Zhang, A. Dutta, C. Han, I. Vincon, A. L. Rogach, A. Nag, A. Samanta, B. A. Korgel, C.-J. Shih, D. R. Gamelin, D. H. Son, H. Zeng, H. Zhong, H. Sun, H. V. Demir, I. G. Scheblykin, I. Mora-Seró, J. K. Stolarczyk, J. Z. Zhang, J. Feldmann, J. Hofkens, J. M. Luther, J. Pérez-Prieto, L. Li, L. Manna, M. I. Bodnarchuk, M. V. Kovalenko, M. B. J. Roeffaers, N. Pradhan, O. F. Mohammed, O. M. Bakr, P. Yang, P. Müller-Buschbaum, P. V. Kamat, Q. Bao, Q. Zhang, R. Krahne, R. E. Galian, S. D. Stranks, S. Bals, V. Biju, W. A. Tisdale, Y. Yan, R. L. Z. Hoye and L. Polavarapu, State of the Art and Prospects for Halide Perovskite Nanocrystals, *ACS Nano*, 2021, **15**(7), 10775–10981, DOI: 10.1021/acsnano.0c08903.

6 B. Chen, P. N. Rudd, S. Yang, Y. Yuan and J. Huang, Imperfections and Their Passivation in Halide Perovskite Solar Cells, *Chem. Soc. Rev.*, 2019, **48**(14), 3842–3867, DOI: 10.1039/C8CS00853A.

7 L. Protesescu, S. Yakunin, M. I. Bodnarchuk, F. Krieg, R. Caputo, C. H. Hendon, R. X. Yang, A. Walsh and M. V. Kovalenko, Nanocrystals of Cesium Lead Halide

 © 2024 The Author(s). Published by the Royal Society of Chemistry

Open Access Article. Published on 19 February 2024. Downloaded on 1/20/2026 12:47:57 PM.
This article is licensed under a Creative Commons Attribution-NonCommercial 3.0 Unported Licence.

Perovskites ($CsPbX_3$, X = Cl, Br, and I): Novel Optoelectronic Materials Showing Bright Emission with Wide Color Gamut, *Nano Lett.*, 2015, **15**(6), 3692–3696, DOI: 10.1021/nl5048779.

8 S. Toso, D. Baranov, C. Giannini, S. Marras and L. Manna, Wide-Angle X-Ray Diffraction Evidence of Structural Coherence in $CsPbBr_3$ Nanocrystal Superlattices, *ACS Mater. Lett.*, 2019, **1**(2), 272–276, DOI: 10.1021/acsmaterialslett.9b00217.

9 M. C. Brennan, S. Toso, I. M. Pavlovetc, M. Zhukovskyi, S. Marras, M. Kuno, L. Manna and D. Baranov, Superlattices Are Greener on the Other Side: How Light Transforms Self-Assembled Mixed Halide Perovskite Nanocrystals, *ACS Energy Lett.*, 2020, **5**(5), 1465–1473, DOI: 10.1021/acsenergylett.0c00630.

10 N. Yazdani, M. Jansen, D. Bozyigit, W. M. M. Lin, S. Volk, O. Yarema, M. Yarema, F. Juranyi, S. D. Huber and V. Wood, Nanocrystal Superlattices as Phonon-Engineered Solids and Acoustic Metamaterials, *Nat. Commun.*, 2019, **10**(1), 4236, DOI: 10.1038/s41467-019-12305-3.

11 J. Hallstrom, I. Cherniukh, X. Zha, M. V. Kovalenko and A. Travesset, Ligand Effects in Assembly of Cubic and Spherical Nanocrystals: Applications to Packing of Perovskite Nanocubes, *ACS Nano*, 2023, **17**(8), 7219–7228, DOI: 10.1021/acsnano.2c10079.

12 I. Cherniukh, G. Rainò, T. V. Sekh, C. Zhu, Y. Shynkarenko, R. A. John, E. Kobiyama, R. F. Mahrt, T. Stöferle, R. Erni, M. V. Kovalenko and M. I. Bodnarchuk, Shape-Directed Co-Assembly of Lead Halide Perovskite Nanocubes with Dielectric Nanodisks into Binary Nanocrystal Superlattices, *ACS Nano*, 2021, **15**(10), 16488–16500, DOI: 10.1021/acsnano.1c06047.

13 I. Cherniukh, T. V. Sekh, G. Rainò, O. J. Ashton, M. Burian, A. Travesset, M. Athanasiou, A. Manoli, R. A. John, M. Svyrydenko, V. Morad, Y. Shynkarenko, F. Montanarella, D. Naumenko, H. Amenitsch, G. Itskos, R. F. Mahrt, T. Stöferle, R. Erni, M. V. Kovalenko and M. I. Bodnarchuk, Structural Diversity in Multicomponent Nanocrystal Superlattices Comprising Lead Halide Perovskite Nanocubes, *ACS Nano*, 2022, **16**(5), 7210–7232, DOI: 10.1021/acsnano.1c10702.

14 I. Cherniukh, G. Rainò, T. Stöferle, M. Burian, A. Travesset, D. Naumenko, H. Amenitsch, R. Erni, R. F. Mahrt, M. I. Bodnarchuk and M. V. Kovalenko, Perovskite-Type Superlattices from Lead Halide Perovskite Nanocubes, *Nature*, 2021, **593**(7860), 535–542, DOI: 10.1038/s41586-021-03492-5.

15 D. Lapkin, C. Kirsch, J. Hiller, D. Andrienko, D. Assalauova, K. Braun, J. Carnis, Y. Y. Kim, M. Mandal, A. Maier, A. J. Meixner, N. Mukharamova, M. Scheele, F. Schreiber, M. Sprung, J. Wahl, S. Westendorf, I. A. Zaluzhnyy and I. A. Vartanyants, Spatially Resolved Fluorescence of Caesium Lead Halide Perovskite Supercrystals Reveals Quasi-Atomic Behavior of Nanocrystals, *Nat. Commun.*, 2022, **13**(1), 892, DOI: 10.1038/s41467-022-28486-3.

16 D. Baranov, A. Fieramosca, R. X. Yang, L. Polimeno, G. Lerario, S. Toso, C. Giansante, M. D. Giorgi, L. Z. Tan, D. Sanvitto and L. Manna, Aging of Self-Assembled Lead Halide Perovskite Nanocrystal Superlattices: Effects on Photoluminescence and Energy Transfer, *ACS Nano*, 2021, **15**(1), 650–664, DOI: 10.1021/acsnano.0c06595.

17 P. B. Green, O. S. Lecina, P. P. Albertini, A. Loiudice and R. Buonsanti, Colloidal-ALD-Grown Metal Oxide Shells Enable the Synthesis of Photoactive Ligand/Nanocrystal Composite Materials, *J. Am. Chem. Soc.*, 2023, **145**(14), 8189–8197, DOI: 10.1021/jacs.3c01439.

18 A. Loiudice, M. Strach, S. Saris, D. Chernyshov and R. Buonsanti, Universal Oxide Shell Growth Enables in Situ Structural Studies of Perovskite Nanocrystals during the Anion Exchange Reaction, *J. Am. Chem. Soc.*, 2019, **141**(20), 8254–8263, DOI: 10.1021/jacs.9b02061.

19 A. Loiudice, O. Segura Lecina, A. Bornet, J. M. Luther and R. Buonsanti, Ligand Locking on Quantum Dot Surfaces via a Mild Reactive Surface Treatment, *J. Am. Chem. Soc.*, 2021, **143**(33), 13418–13427, DOI: 10.1021/jacs.1c06777.

20 A. Loiudice, O. Segura Lecina and R. Buonsanti, Atomic Control in Multicomponent Nanomaterials: When Colloidal Chemistry Meets Atomic Layer Deposition, *ACS Mater. Lett.*, 2020, **2**(9), 1182–1202, DOI: 10.1021/acsmaterialslett.0c00271.

21 P. Green, O. S. Lecina, P. Albertini, M. Newton, K. Kumar, C. Boulanger, J. Leemans, P. Thompson, A. Loiudice and R. Buonsanti, Colloidal Atomic Layer Deposition on Nanocrystals Using Ligand-Modified Precursors, PREPRINT Reseach Square, 2024, DOI: 10.21203/rs.3.rs-3792425/v1.

22 P. P. Albertini, M. A. Newton, M. Wang, O. S. Lecina, P. B. Green, D. C. Stoian, E. Oveisi, A. Loiudice and R. Buonsanti, Hybrid oxide coatings generate stable Cu catalysts for CO_2 electroreduction, *Nat. Mater.*, 2024, DOI: 10.1038/s41563-024-01819-x.

23 S. C. Boehme, M. I. Bodnarchuk, M. Burian, F. Bertolotti, I. Cherniukh, C. Bernasconi, C. Zhu, R. Erni, H. Amenitsch, D. Naumenko, H. Andrusiv, N. Semkiv, R. A. John, A. Baldwin, K. Galkowski, N. Masciocchi, S. D. Stranks, G. Rainò, A. Guagliardi and M. V. Kovalenko, Strongly Confined $CsPbBr_3$ Quantum Dots as Quantum Emitters and Building Blocks for Rhombic Superlattices, *ACS Nano*, 2023, **17**(3), 2089–2100, DOI: 10.1021/acsnano.2c07677.

24 C. K. Ng, W. Yin, H. Li and J. J. Jasieniak, Scalable Synthesis of Colloidal $CsPbBr_3$ Perovskite Nanocrystals with High Reaction Yields through Solvent and Ligand Engineering, *Nanoscale*, 2020, **12**(8), 4859–4867, DOI: 10.1039/C9NR10726F.

25 J. J. Choi, C. R. Bealing, K. Bian, K. J. Hughes, W. Zhang, D.-M. Smilgies, R. G. Hennig, J. R. Engstrom and T. Hanrath, Controlling Nanocrystal Superlattice Symmetry and Shape-Anisotropic Interactions through Variable Ligand Surface Coverage, *J. Am. Chem. Soc.*, 2011, **133**(9), 3131–3138, DOI: 10.1021/ja110454b.

26 J. Liu, X. Zheng, O. F. Mohammed and O. M. Bakr, Self-Assembly and Regrowth of Metal Halide Perovskite Nanocrystals for Optoelectronic Applications, *Acc. Chem. Res.*, 2022, **55**(3), 262–274, DOI: 10.1021/acs.accounts.1c00651.

Open Access Article. Published on 19 February 2024. Downloaded on 1/20/2026 12:47:57 PM.
This article is licensed under a Creative Commons Attribution-NonCommercial 3.0 Unported Licence.

27 S. Yakunin, L. Protesescu, F. Krieg, M. I. Bodnarchuk, G. Nedelcu, M. Humer, G. De Luca, M. Fiebig, W. Heiss and M. V. Kovalenko, Low-Threshold Amplified Spontaneous Emission and Lasing from Colloidal Nanocrystals of Caesium Lead Halide Perovskites, *Nat. Commun.*, 2015, **6**(1), 8056, DOI: 10.1038/ncomms9056.

28 S. Toso, D. Baranov, U. Filippi, C. Giannini and L. Manna, Collective Diffraction Effects in Perovskite Nanocrystal Superlattices, *Acc. Chem. Res.*, 2023, **56**(1), 66–76, DOI: 10.1021/acs.accounts.2c00613.

29 S. Toso, D. Baranov, D. Altamura, F. Scattarella, J. Dahl, X. Wang, S. Marras, A. P. Alivisatos, A. Singer, C. Giannini and L. Manna, Multilayer Diffraction Reveals That Colloidal Superlattices Approach the Structural Perfection of Single Crystals, *ACS Nano*, 2021, **15**(4), 6243–6256, DOI: 10.1021/acsnano.0c08929.

30 Z. Li, P. R. Wray, M. P. Su, Q. Tu, H. P. Andaraarachchi, Y. J. Jeong, H. A. Atwater and U. R. Kortshagen, Aluminum Oxide Nanoparticle Films Deposited from a Nonthermal Plasma: Synthesis, Characterization, and Crystallization, *ACS Omega*, 2020, **5**(38), 24754–24761, DOI: 10.1021/acsomega.0c03353.

31 M. Kaushik, C. Leroy, Z. Chen, D. Gajan, E. Willinger, C. R. Müller, F. Fayon, D. Massiot, A. Fedorov, C. Copéret, A. Lesage and P. Florian, Atomic-Scale Structure and Its Impact on Chemical Properties of Aluminum Oxide Layers Prepared by Atomic Layer Deposition on Silica, *Chem. Mater.*, 2021, **33**(9), 3335–3348, DOI: 10.1021/acs.chemmater.1c00516.

32 M. I. Bodnarchuk, S. C. Boehme, S. Ten Brinck, C. Bernasconi, Y. Shynkarenko, F. Krieg, R. Widmer, B. Aeschlimann, D. Günther, M. V. Kovalenko and I. Infante, Rationalizing and Controlling the Surface Structure and Electronic Passivation of Cesium Lead Halide Nanocrystals, *ACS Energy Lett.*, 2019, **4**(1), 63–74, DOI: 10.1021/acsenergylett.8b01669.

33 N. Soetan, W. R. Erwin, A. M. Tonigan, D. G. Walker and R. Bardhan, Solvent-Assisted Self-Assembly of $CsPbBr_3$ Perovskite Nanocrystals into One-Dimensional Superlattice, *J. Phys. Chem. C*, 2017, **121**(33), 18186–18194, DOI: 10.1021/acs.jpcc.7b03939.

34 M. Palei, M. Imran, G. Biffi, L. Manna, F. Di Stasio and R. Krahne, Robustness to High Temperatures of Al_2O_3-Coated $CsPbBr_3$ Nanocrystal Thin Films with High-Photoluminescence Quantum Yield for Light Emission, *ACS Appl. Nano Mater.*, 2020, **3**(8), 8167–8175, DOI: 10.1021/acsanm.0c01525.

35 S. Saris, S. T. Dona, V. Niemann, A. Loiudice and R. Buonsanti, Optimizing the Atomic Layer Deposition of Alumina on Perovskite Nanocrystal Films by Using O_2 As a Molecular Probe, *Helv. Chim. Acta*, 2020, **103**(6), e2000055, DOI: 10.1002/hlca.202000055.

36 X. Du, G. Wu, J. Cheng, H. Dang, K. Ma, Y.-W. Zhang, P.-F. Tan and S. Chen, High-Quality $CsPbBr_3$ Perovskite Nanocrystals for Quantum Dot Light-Emitting Diodes, *RSC Adv.*, 2017, **7**(17), 10391–10396, DOI: 10.1039/C6RA27665B.

 © 2024 The Author(s). Published by the Royal Society of Chemistry